Materials Research Express

PAPER

Structure and properties of ZnS_xSe_{1-x} thin films deposited by thermal evaporation of ZnS and ZnSe powder mixtures

RECEIVED
3 June 2014

ACCEPTED FOR PUBLICATION
22 December 2014

PUBLISHED
26 January 2015

R G Valeev[1], E A Romanov[2], V L Vorobiev[1], V V Mukhgalin[1], V V Kriventsov[3], A I Chukavin[1] and B V Robouch[4]

[1] Physical-Technical Institute of Ural Brunch of RAS, Kirova str. 132, Izhevsk 426000, Russia
[2] Udmurt State University, Universitetskaya str. 1, Izhevsk 426034, Russia
[3] Boreskov's Institute of Catalysis of Siberian Brunch of RAS, Lavrentieva 5, Novosibirsk 630090, Russia
[4] Istituto Nazionale di Fisica Nucleare-Laboratori Nazionali di Frascati, Via E. Fermi 40, I-00044 Frascati, Italy

E-mail: rishatvaleev@mail.ru

Keywords: thin films of ZnS_xSe_{1-x} compounds, thermal evaporation of ZnS and ZnSe powders mixture, EXAFS spectroscopy, x-ray diffraction, Raman spectroscopy, band gap

Abstract

Interest to ZnS_xSe_{1-x} alloys is due to their band-gap tunability varying S and Se content. Films of ZnS_xSe_{1-x} were grown evaporating ZnS and ZnSe powder mixtures onto SiO_2, NaCl, Si and ITO substrates using an original low-cost method. X-ray diffraction patterns and Raman spectroscopy, show that the lattice structure of these films is cubic ZnSe-like, as S atoms replace Se and film compositions have their initial S/Se ratio. Optical absorption spectra show that band gap values increase from 2.25 to 3 eV as *x* increases, in agreement with the literature. Because S atomic radii are smaller than Se, EXAFS spectra confirm that bond distances and Se coordination numbers decrease as the Se content decreases. The strong deviation from linearity of ZnSe coordination numbers in the ZnS_xSe_{1-x} indicate that within this ordered crystal structure strong site occupation preferences occur in the distribution of Se and S ions. The behavior is quantitatively confirmed by the strong deviation from the random Bernoulli distribution of the three sight occupation preference coefficients of the strained tetrahedron model. Actually, the ternary ZnS_xSe_{1-x} system is a bi-binary (ZnS+ZnSe) alloy with evanescent formation of ternary configurations throughout the *x*-range.

1. Introduction

The achievements in semiconductor technology during the second half of the 1970s led to 'band gap engineering'—the formation of semiconductors with tunable band gaps. In fact, the output wavelength of optoelectronic devices is strongly linked to band gap energy [1]. Recently, ZnS_xSe_{1-x} ternary alloys have been extensively studied because their emission wavelength can be tuned gradually by increasing *x* in the alloy. Tang *et al* [2] reported that increasing the S to Se relative content from 0 to 100% led to a decrease in the excitation and emission wavelengths from 465 to 340 nm and from 644 to 505 nm, respectively. The color of emission also changed from red to green. ZnS_xSe_{1-x} compounds are also widely used in place of CdS as buffer-layer material for $Cu(In,Ga)Se_2$ (CIGS) thin-film solar cells [3]. These compounds are also used in the fabrication of blue-green laser diodes [4] and electroluminescent light emitting panels [5].

The ZnS_xSe_{1-x} thin films were prepared by the molecular beam epitaxy (MBE) process [1, 2, 4, 6], laser ablation [7], chemical and physical vapor deposition [8, 9], and chemical bath deposition [10]. In [9] the ZnS and ZnSe powders were thoroughly mixed in proportions providing the concentration of S and Se in the ZnS_xSe_{1-x} films and deposited on a substrate by close-spaced evaporation. The method used in [9] is similar to the conventional thermal deposition technique, but more complex. Ashraf *et al* [11] report results of optical and structural properties of thin ZnS_xSe_{1-x} films obtained by thermal evaporation of ZnS and ZnSe powders mixture on glass substrate using a complex and expensive setup.

© 2015 IOP Publishing Ltd

We describe a novel, simple method of thermal deposition for ternary compounds using low cost experimental equipment [12]. We report the results on the structural and optical properties of ZnS_xSe_{1-x} films deposited on different substrates, namely quartz, indium tin oxide (ITO), NaCl, and Si. The desired content of sulfur and selenium in the ZnS_xSe_{1-x} films was obtained by mixing appropriate amounts of ZnS and ZnSe powders. This method was used for the first time to deposit ZnS_xSe_{1-x} films and can subsequently be used to deposit ZnS_xSe_{1-x} onto porous anodic alumina in creating nanostructures [13, 14]. The structure was studied by x-ray diffraction (XRD) and Raman spectroscopy. Surface images were obtained by scanning electron microscopy (SEM). Optical band gaps and their function of x have also been calculated using standard methods and formulae [15].

The local atomic structure was investigated using the extended x-ray absorption fine structure (EXAFS) method. The method was used earlier to determine the parameters of the local atomic environment of ZnS [16], ZnSe [12] and of $ZnS_{0.06}Se_{0.94}$ [17] thin films. EXAFS is powerful, but its accuracy is strongly affected by several factors, such as sample quality, k-range, data acquisition and, of course, treatment [18, 19]. To extract all relevant parameters from EXAFS spectra, a sufficient amount of experimental data is required by the strained tetrahedron model [20]. The model then allows retrieving besides the three SOP coefficients, the component configurations of nearest neighbor (NN) and next nearest neighbor (NNN) observations of zincblende/sphalerite and wurtzite ZnS structured crystalline materials, namely bond-distances and inter bond-angles [20–23]. The strained tetrahedron model was successfully used to analyze EXAFS and neutron-scatter data of twenty-two different datasets of ternary alloys covering eighteen B3, B4, $L1_2$, and C15 structures [22]. Successively, the statistical model [23, 24] was developed to analyze far infrared (FIR) spectra [25]. Analysis of independent EXAFS and FIR data for a given alloy yields the same deviations from Bernoulli binomial distributions.

The data here collected allows determining besides the three SOP coefficients, the Zn-Se bond distance of the $^3T_1$ configuration, while extreme site occupation preferences prevent the formation of configurations $^2T_2$ and $^1T_3$.

2. Experimental details

ZnS_xSe_{1-x} films with $x = 0.36$, 0.68 and 0.73 were synthesized by using explosive thermal evaporation: powder is strewn from a vibrating bin to a molybdenum crucible heated to 1500 °C., and is then evaporated and condensed on substrates [12]. The films were deposited on cleaned quartz, indium tin oxide (ITO), NaCl and Si substrates kept at a temperature of 200 °C in a vacuum of 10^{-6} Pa. Pure ZnS and ZnSe powders were mixed according to the mass proportions of 1:3, 1:1 and 3:1. The calculated S/Se ratio in ZnS_xSe_{1-x} with relative contents [13], correspond to 1:3, 1:1 and 3:1 ZnS and ZnSe mass ratios, respectively.

The chemical compositions of the deposited films were tested by secondary mass ion spectroscopy (SIMS) and result in $ZnS_{0.36}Se_{0.64}$, $ZnS_{0.68}Se_{0.32}$ and $ZnS_{0.73}Se_{0.27}$ regardless of the substrate material. The film compositions were in good agreement with the S/Se ratio in ZnS and ZnSe powder mixtures. The thicknesses of the films, measured by optical interference were about 150 nm.

XRD patterns were recorded in the 2θ range of 15–65° by a BRUKER D8 advance x-ray diffractometer with Cu-$K\alpha$ radiation. Registration was carried out in grazing incidence angle mode using a single Gobel mirror, with an incident angle of 1°. A Si(Li) solid-state detector was used to detect x-ray radiation.

Scanning electron microscopy images were obtained on a Supra LEO microscope under the accelerating voltage of 5 kV and magnification of 50 000. An illustrative image is given (figure 2). The Raman spectra were recorded by using a Renishaw InVia Raman microscope under Ar^+ (514 nm) laser excitation in the range 100–600 cm^{-1}. The UV–vis absorption spectra were recorded on a Perkin-Elmer Lambda 950 UV–vis spectrometer in the range 250–1000 nm.

The local atomic structure was studied by EXAFS spectroscopy at the Siberian Synchrotron Radiation Center (SSRC), Novosibirsk. The VEPP-3 storage ring (with an electron beam energy of 2 GeV and average stored current of 80 mA) was used as the radiation source. The x-ray energy was monitored with a channel cut Si(111) monochromator. The spectra were recorded under the fluorescent mode at Zn K-edge ($E_K = 9660$ eV) and Se K-edge ($E_K = 12\,658$ eV), with a step of 1.5 eV. For the harmonic rejection, a SiO_2 mirror was used for all measurements.

3. Results and discussion

The XRD study was performed on samples deposited on SiO_2 substrate. Figure 1 shows films that have good crystallinity with the sphalerite (111) texture. There are significant shifts of the (111) peaks for the films with different S/Se ratios, which can be associated with changes of the lattice parameter value [26, 11]. Thus, the pure ZnSe has (111) the peak position at 27.29° (JCPDS # 01-071-5977), whereas for $ZnS_{0.36}Se_{0.64}$ the peak is shifted

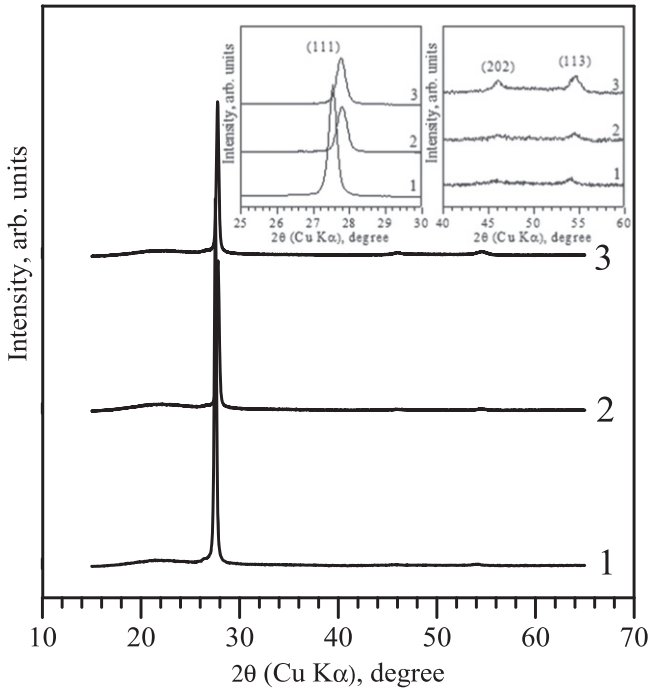

Figure 1. XRD spectra of ZnS_xSe_{1-x} films on SiO_2 substrate: $ZnS_{0.36}Se_{0.64}$ (curve 1), $ZnS_{0.68}Se_{0.32}$ (curve 2) and $ZnS_{0.73}Se_{0.27}$ (curve 3).

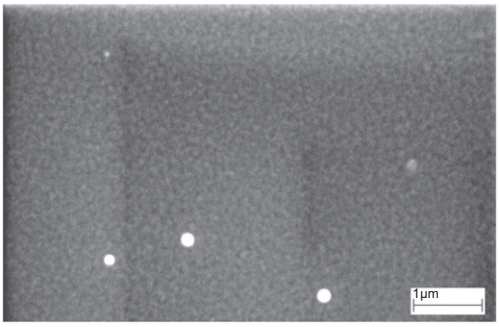

Figure 2. SEM-image of a $ZnS_{0.73}Se_{0.27}$ film on a Si substrate.

to 27.54°, for $ZnS_{0.68}Se_{0.32}$ to 27.8° and for $ZnS_{0.73}Se_{0.27}$ to 27.84°. Pure ZnS has (111) a peak position at 28.63° (JCPDS # 01-071-5975). The right inset in the figure shows that the (202) and (113) peaks are shifted to higher values. The lattice structure does not change and remains a cubic ZnSe-like sphalerite structure while sulfur atoms occupy selenium sites within the lattice during film formation.

An SEM image of the surface of a $ZnS_{0.73}Se_{0.27}$ film deposited on a silicon substrate is shown (figure 2). The surface morphology of films deposited on the NaCl, ITO and SiO_2 substrates are practically identical and show a coating, consisting of small (about 2–10 nm in diameter) particles. It is natural for films obtained by thermal deposition method [27].

Figure 3 represents the Raman spectra of $ZnS_{0.73}Se_{0.27}$ films deposited on the NaCl, ITO, SiO_2 and Si substrates. The studies indicated that the substrate materials did not influence the shape or position of the ZnSe-like and ZnS-like peaks. Raman spectra of $ZnS_{0.36}Se_{0.64}$, $ZnS_{0.68}Se_{0.32}$ and $ZnS_{0.73}Se_{0.27}$ films are compared to the spectra for the ZnS and ZnSe films (figure 4). ZnSe-like longitudinal and transverse optical (LO and TO, respectively) modes come closer to each other with increasing sulfur content. At the same time the ZnS-like LO peak is shifted towards higher frequencies. Similar results were reported in [28] for tetrapod-like ZnS_xSe_{1-x} alloy nanostructures and are in good agreement with the theoretical predictions of the modified random element isodisplacement model [29].

Figure 4 also shows the asymmetry of the ZnS-like LO mode peaks towards lower frequencies. This asymmetry can be explained by the fact that during the film formation, sulfur atoms replace selenium atoms in

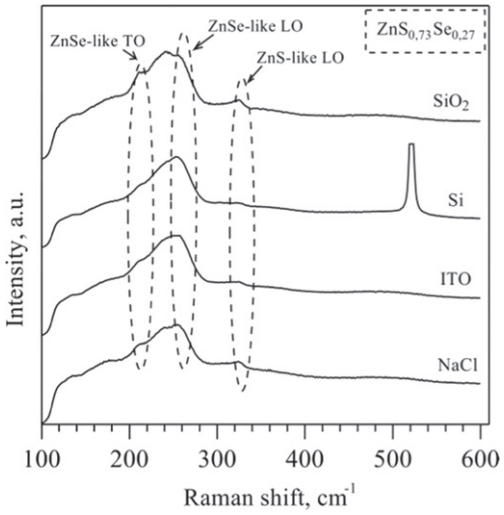

Figure 3. Raman spectra of $ZnS_{0,73}Se_{0,27}$ films deposited on SiO_2, Si, ITO and NaCl substrates.

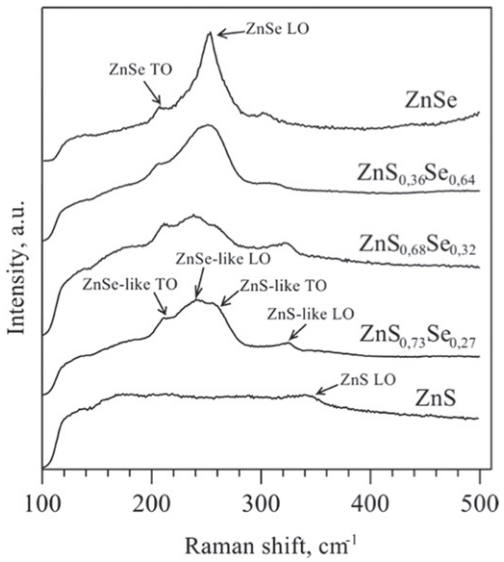

Figure 4. Raman spectra for $ZnS_{0.36}Se_{0.64}$, $ZnS_{0.68}Se_{0.32}$, $ZnS_{0.73}Se_{0.27}$, ZnS and ZnSe.

the lattice and it is not known which selenium atom in the lattice was replaced. It should be noted that in contrast to the other results of the Raman investigation (see, e.g., [29, 30]), ZnS-like TO mode peaks were observed. The positions of these peaks were not shifted with the change in film composition, and for the $ZnS_{0.36}Se_{0.64}$ film the ZnS-like TO mode peak merges with ZnSe-like LO mode peak.

Optical transmittance coefficient T versus wavelength measurements were used to carry out optical studies on ZnS_xSe_{1-x} films deposited on SiO_2 substrates. Figure 5(a) shows the transmittance spectra of $ZnS_{0.36}Se_{0.64}$, $ZnS_{0.68}Se_{0.37}$ and $ZnS_{0.73}Se_{0.27}$ films. Optical energy band gap values were determined by the method described in [15]. The experimental data near the edge of an absorption level can be described for crystalline films by

$$|\sigma(\omega)\hbar\omega|^2 = A^2\left(\hbar\omega - E_g\right), \quad (1)$$

where $\sigma(\omega)$ is the absorption coefficient (determined from the experimental data), $\hbar\omega = 2\pi\hbar c/\lambda$ is the photons energy, E_g is the band gap value, while A is a constant. In an ideal case the optical energy band gap of the films can be determined by extrapolating the linear portion of the experimental data presenting $[\sigma(\omega)\hbar\omega]^2$ versus the energy (figure 5(b)). The evaluated energy band gap of the films varied in the range 2.25–3.0 eV with the increase in sulfur composition and is summarized in table 1.

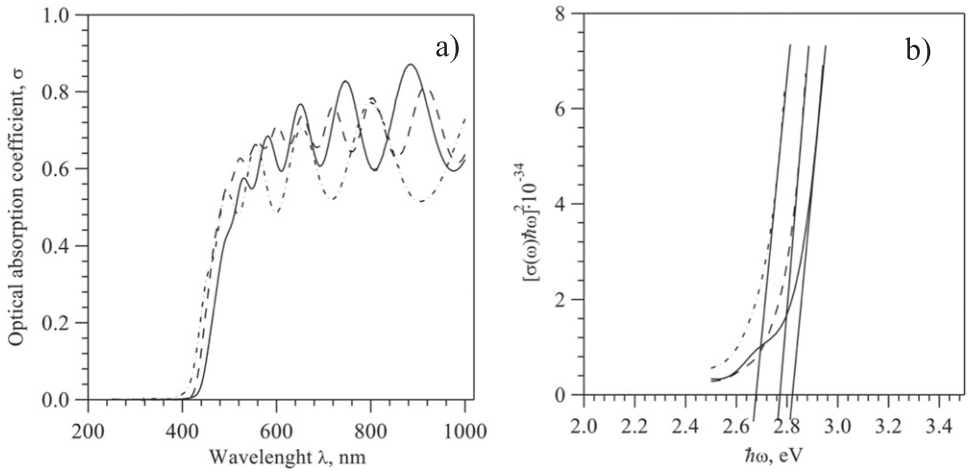

Figure 5. Absorption spectra (a) and dependence of $[\sigma(\omega)\hbar\omega]^2(\hbar\omega)$ (b) for ZnS_xSe_{1-x} thin films ($x = 0.73$—solid line, $x = 0.68$—dashed line and $x = 0.36$—dash-and-dot line).

Table 1. Experimental values of band gaps for ZnSe, $ZnS_{0.36}Se_{0.64}$, $ZnS_{0.68}Se_{0.32}$, $ZnS_{0.73}Se_{0.27}$ and ZnS, Eg values calculated [1] versus experimental values.

ZnS_xSe_{1-x} Composition	E_g calculation [1]	Experimental E_g value
ZnS	3.7	3 [31]
$ZnS_{0.73}Se_{0.27}$	3.24	2.82
$ZnS_{0.68}Se_{0.32}$	3.19	2.77
$ZnS_{0.36}Se_{0.64}$	2.92	2.68
ZnSe	2.77	2.25 [12]

The dependence of the energy gap of a ternary $A^{II}B^{VI}C^{VI}$ alloy on the composition x at a fixed temperature can be described by the empirical equation [32]:

$$E_g(x) = xE_g^{BC} + (1 - x)E_g^{AC} - bx(1 - x) \quad (2)$$

where E_g^{BC} and E_g^{AC} are the fundamental band gaps of the binary compounds and b is the parameter of optical mismatch (or 'bowing' parameter). For ZnS_xSe_{1-x} $E_g^{ZnS} = 3.7$ eV and $E_g^{ZnSe} = 2.77$ eV, with $E_g(x)$ calculated [1]:

$$E_g = 2.77 + 0.21x + 0.6x^2 \quad (3)$$

The variation in band gap with composition is found to be nonlinear, showing a similar bowing; the degree of nonlinearity can be fitted to the following quadratic equation:

$$E_g = 2.25 + 0.21x + 0.6x^2 \quad (4)$$

The significant decrease in the experimental band gap values compared to the fundamental values is probably caused by the formation of extra Tamm bands in the gap due to the significant influence of film/substrate interface. Tamm showed that in contrast to the situation in the bulk crystal, localized states can appear on the surface that consist of structural defects, atoms, and molecules adsorbed from the environment, among others. This leads, as mentioned above, to a decrease in the band gap. The results obtained are in good agreement with values presented, for example, by Ashraf *et al* [11].

Figures 6 and 7 show the normalized oscillatory parts (NOP) and their Fourier-transforms (FT) for EXAFS spectra recorded on Se and Zn K-edges for the ZnSe, $ZnS_{0.36}Se_{0.64}$, $ZnS_{0.68}Se_{0.37}$ and $ZnS_{0.73}Se_{0.27}$ films. The parameters of the local atomic structure calculated by the Fourier fitting procedure are summarized in table 1.

It can be seen (figure 6) that the increase in the selenium contents (i.e., concentration of the scattering atoms) led to an increase in the NOPs amplitudes. For $ZnS_{0.36}Se_{0.64}$, $ZnS_{0.68}Se_{0.37}$, and $ZnS_{0.73}Se_{0.27}$ films, the well-defined peaks attributed to the first coordination sphere and the highly diffuse peaks attributed to the second coordination sphere can be seen in figure 7. Table 1 shows that with decreasing selenium content the values of bond distances and Se coordination numbers also decrease (figures 8(c), (d)). The concentration of

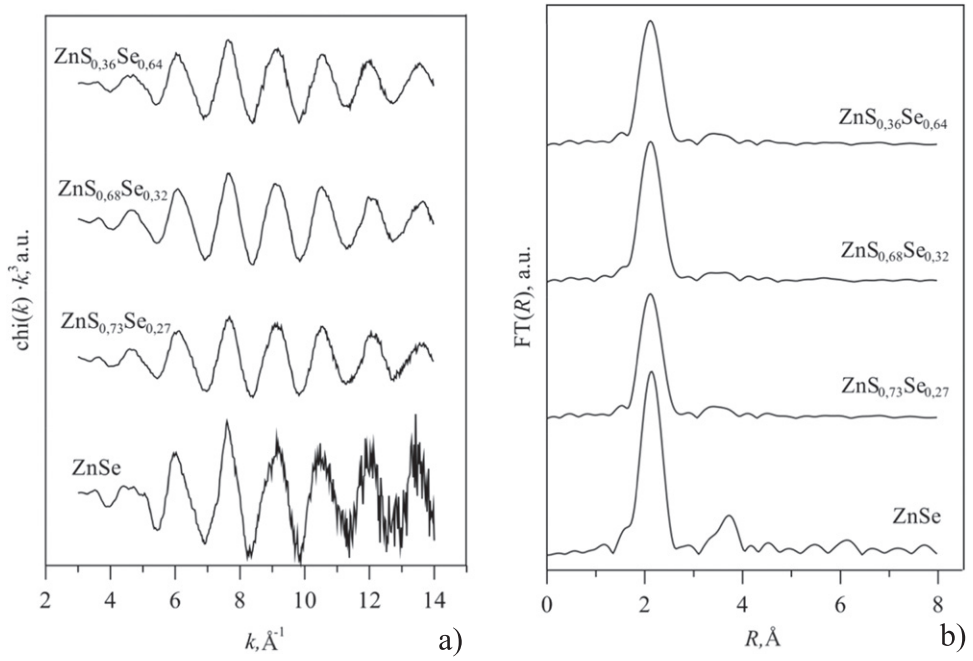

Figure 6. Normalized oscillation parts (a) and Fourier transforms (b) of Se K-edge EXAFS-spectra.

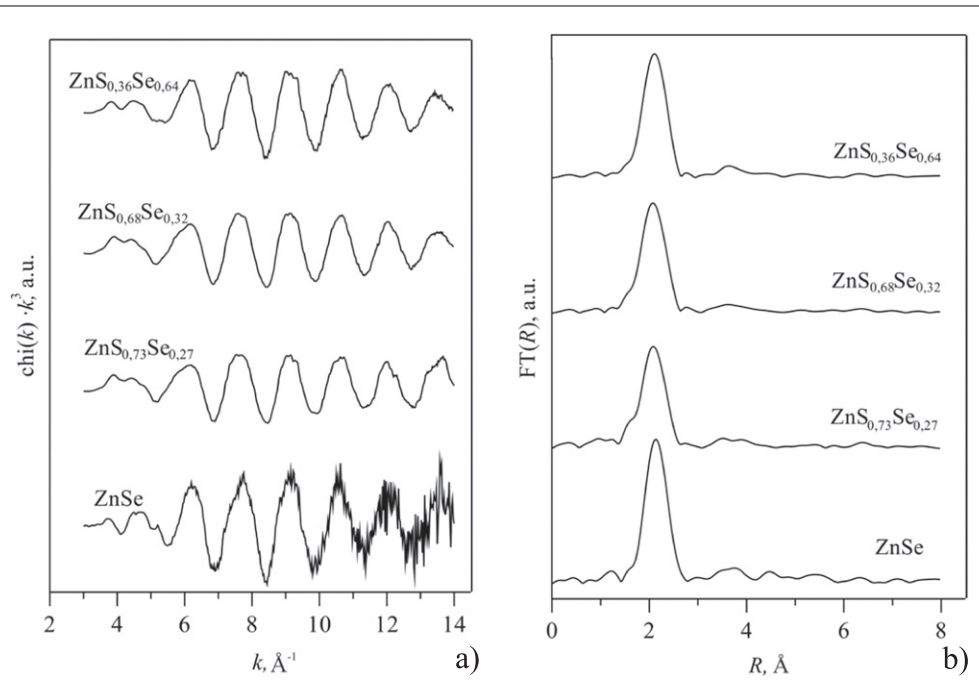

Figure 7. Normalized oscillation parts (a) and Fourier transforms (b) of Zn K-edge EXAFS-spectra.

scattering atoms diminishes as sulfur atoms with smaller atomic radius replace selenium atoms. This leads to a decrease in the bond distances between selenium and its neighbors (Zn, Se and S), a decrease in the coordination number (CN) in the Se–Se atomic pair and, as noted above, a shift of the XRD reflections to higher values. At the same time, the CN for the Zn-Zn atomic pair increases with the increase in the sulfur content. This is also connected to the fact that sulfur atoms replace selenium atoms with higher atomic radius. Zinc atoms come closer to each other and more readily participate in the formation of the coordination sphere.

The EXAFS observations of ZnS_xSe_{1-x} coordination numbers and bond-distances of both NN and NNN at three $x_S = [0.36, 0.68, 0.73]$ values are shown (table 2).

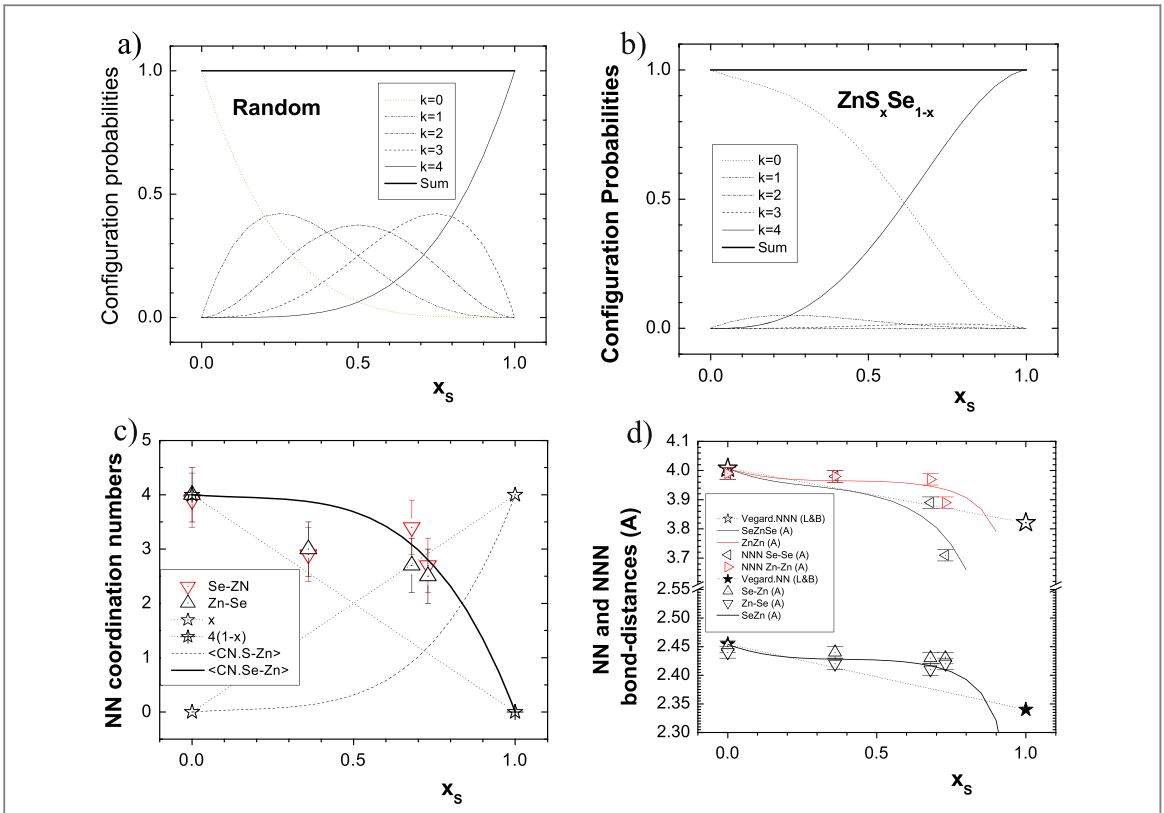

Figure 8. Graphical results of the strained tetrahedron model analysis of our ZnS_xSe_{1-x} EXAFS experimental observations: (a) Random configuration probabilities versus x_S, (b) ZnS_xSe_{1-x} configuration probabilities versus x_S, (c) NN coordination numbers ZnSe and ZnS versus x_S, (d) Bond-distances (Å) NN ZnSe and NNN ZnZn and SeSe versus x_S.

Table 2. Bond distances (R) and coordination numbers (N) obtained by Fourier transform method for atomic pairs Zn–Zn, Zn–Se, Se–Zn and Se–Se, where subscripts 1 and 2 refer to the coordination shell, respectively NN and NNN.

	Se–Zn		Se–Se	Zn–Se		Zn–Zn
	R_1, Å	CN_1	R_2, Å	R_1, Å	CN_1	R_2, Å
Crystallographic model	2.450	4	4.00	2.450	4	4.00
ZnSe	2.45 ± 0.01	3.9 ± 0.5	3.99 ± 0.02	2.44 ± 0.01	4.0 ± 0.5	3.99 ± 0.02
$ZnS_{0.36}Se_{0.64}$	2.44 ± 0.01	2.9 ± 0.5	3.98 ± 0.02	2.42 ± 0.01	3.0 ± 0.5	3.98 ± 0.02
$ZnS_{0.68}Se_{0.32}$	2.43 ± 0.01	3.4 ± 0.5	3.89 ± 0.02	2.41 ± 0.01	2.7 ± 0.5	3.97 ± 0.02
$ZnS_{0.73}Se_{0.27}$	2.43 ± 0.01	2.7 ± 0.5	3.71 ± 0.02	2.42 ± 0.01	2.5 ± 0.5	3.89 ± 0.02

The 150 nm thick film, with lattice parameters $a_{ZnSe} = 0.567$ nm and $a_{ZnS} = 0.541$ nm, contains ~300 layers. We may then consider the film growth to have a prevalently ordered crystal structure. A best fit of the whole set of point values can then be achieved using the strained tetrahedron model [20].

The strained tetrahedron model assumes that canonically a B3, B4, $L1_2$ tetrahedron structure, hence that of sphalerite ZnS_xSe_{1-x}, consists of five tetrahedron configurations $\{^{4-k}T_k\}_{k=0,4}$ (where $^4T_0$ and $^0T_4$ are binary ZnSe and ZnS, respectively, while the remaining three configurations are ternary since each contains all three atoms Zn, Se, and S). The tetrahedron configurations imply three SOP coefficients, and nineteen elemental ternary bond distance parameters (six NN and thirteen NNN); tetrahedron constraints reduce the bond-distance degrees of freedom to ten [20]. Thus, to allow a best-fit analysis of a complete tetrahedron structure with thirteen free parameters (NN and NNN), at least fourteen observed data are required, as in our case (table 2). In a zinc-blend alloy with no site occupation preferences (SOPs) all atoms are distributed randomly and are described by Bernoulli binomials (figure 8(a)). In the case of preferences, distributions deviate from Bernoulli values (figure 8(b)). For data best fitting, we used the routine Microsoft Office Excel Resolver with the default Newton method. We underline here that analysis of independent EXAFS and FIR data for a given alloy yields the same deviations from Bernoulli distributions.

A best fit of the experimental observations (table 2) yields the three SOP-coefficient values, i.e. the attenuation with respect to Bernoulli values, one for each of the three ternary configurations: $C_k = [0.12, 0, 0.03]$. Thus, as x_S goes from 0 to 1, the ZnS_xSe_{1-x} evolves without the formation of either $^2T_2$ or $^1T_3$ (figure 4, top right).

Table 3. Strained tetrahedron model analysis experimental observations of ZnS_xSe_{1-x} of table 2.

Tetrahedron configuration	${}^{k}T_k$	${}^{4}T_0$	${}^{3}T_1$	${}^{2}T_2$	${}^{1}T_3$	${}^{0}T_4$
Configuration number	k	0	1	2	3	4
SOP coefficient	$\boldsymbol{C_k}$	—	0.12	0	0.03	—
SOP preference of S over Se atom [20]	W_k	—	0.12	0	1.32	—
Configuration Zn–Se bond distance	${}^{ZnSe}d$	2.454	1.885	—	—	—

From the literature, bond distances of the binary compounds are ${}^{ZnSe}d = 2.454$ Å and ${}^{ZnS}d = 2.342$ Å. The EXAFS observations of ZnS_xSe_{1-x} coordination numbers and bond distances of both NN and NNN at three x values are shown (table 3 and figures 8(c), (d)).

4. Conclusion

Three ZnS_xSe_{1-x} films (x = 0.36, 0.68 and 0.73) were successfully grown by thermal deposition of a mixture of ZnS and ZnSe powders onto four different substrates SiO_2, Si, ITO and NaCl. The film compositions determined by the right choice of mass proportions of ZnS and ZnSe powders showed a good agreement with the S/Se ratio in the initial mixtures defined by SIMS. Both x-ray diffraction and Raman spectroscopy show similar structures for these films deposited on the four different substrates. Moreover, XRD patterns show that the (111) ZnSe-like peaks shift from 27.54° for $ZnS_{0.36}Se_{0.64}$ to 27.84° for $ZnS_{0.73}Se_{0.27}$. As the sulfur content increases, the band gap of the films shifts from 2.25 to 3 eV. We associate the deviation of the experimental values with respect to the calculated ones to energy band deformations induced by significant disturbances of the structure due to the formation of extra Tamm bands in the gap, to the strain induced at the film/substrate interface as well as to the presence of contaminants present in the surface layers once the samples were exposed to air. The band gap value dependence on the sulfur content x has been approximated with an empirical formula (equation (2)) with a bowing parameter of 0.6. Of the three films, $ZnS_{0.68}Se_{0.37}$ and $ZnS_{0.73}Se_{0.27}$ with a 5% difference in content show slightly different behaviors, while $ZnS_{0.36}Se_{0.64}$ with an $x = 0.36$ content strongly deviates in behavior.

The EXAFS analysis applied for the first time to the ZnS_xSe_{1-x} system shows large changes in the ZnSe-like atomic structure versus x. Indeed, the concentration of the scattering atoms decreases as sulfur atoms with their smaller atomic radii replace Se atoms. Raman spectroscopy confirms this behavior and as x increases, the ZnSe-like LO and TO modes move closer to each other, the ZnS-like LO peak shifts towards higher frequencies, i.e., towards the ZnS LO mode position. All data indicate that these ZnS_xSe_{1-x} ternary films grew with a homogenous composition.

Regarding the anomalous behavior of this ternary composition, we have to consider that for a ternary alloy with no SOPs all atoms are randomly distributed and their distribution can be described by Bernoulli binomials. Observed EXAFS data of zinc-blend structured ZnS_xSe_{1-x}, coordination numbers and bond-distances of NN and NNN, analyzed using the strained tetrahedron model under the assumption of an ordered crystal structure with negligible amorphous phases, indicate a different behavior. The best fit of the experimental spectra yields three SOP-coefficient values with a clear attenuation with respect to the random Bernoulli values, one for each of the three ternary configurations. For the ZnS_xSe_{1-x} the three SOP coefficients $\{C_k\}_{k=1,3}$ turn out to be $C_k = [0.12, 0, 0.03]$, i.e. throughout the $x = [0;1]$ range, the ternary ZnS_xSe_{1-x} system is essentially a bi-binary (ZnS+ZnSe) alloy with an evanescent formation of the ternary configuration ${}^{3}T_1$, while ${}^{2}T_2$ and ${}^{1}T_3$ are not present.

Acknowledgments

The authors wish to acknowledge the Ural Branch of Russian Academy of Sciences for financial support (Projects # 12-S-2-1024 and 12-P-2-1038), RFBR (12-03-01039), Presidium RAS (program 24) and pleasant discussions with Augusto Marcelli.

References

[1] Ben Fredj A, Debbichi M and Said M 2007 Influence of the composition fluctuation and the disorder on the bowing band gap in semiconductor materials *Microelectron. J.* **38** 860–70
[2] Tang T P, Wang W L and Wang S F 2009 The luminescence characteristics of ZnS_xSe_{1-x} phosphor powder *J. Alloys Compd.* **488** 250–3
[3] Jackson P, Hariskos D, Lotter E, Paetel S, Wuerz R, Menner R, Wischmann W and Powalla M 2011 New world record efficiency for Cu (In,Ga)Se_2 thin-film solar cells beyond 20% *Prog. Photovolt., Res. Appl.* **19** 894–7
[4] Prior K 1993 II–VI compounds & related optoelectronic materials *III-Vs Rev.* **6** 42–5
[5] Ichino K, Onishi T, Kawakami Y, Fujita S and Fujita S 1993 Near-UV electroluminescence from a ZnCdSSe/ZnSSe metal-insulator-semiconductor diode on GaP grown by molecular beam epitaxy *Japan. J. Appl. Phys.* 2 **32** L1200–2

[6] Lee M-K, Shih T-H and Tsay B-T 2003 Epitaxial growth of high-quality ZnSSe on ZnSSe/In/glass substrate *Semicond. Sci. Technol.* **18** 1030–2

[7] Ambrico M, Perna G, Smaldone D, Spezzacatena C, Stagno V and Capozzi V 1998 Structural and optical parameters of films deposited on quartz substrates by laser ablation *Semicond. Sci. Technol.* **13** 1446–55

[8] Kumar V and Sharma T P 1998 Structural and optical properties of sintered ZnS_xSe_{1-x} films *Opt. Mater.* **10** 253–6

[9] Subbaiah Y P V, Prathap P, Reddy K T R, Mangalaraj D, Kim K and Yi J 2007 Growth and characterization of ZnS_xSe_{1-x} films deposited by close-spaced evaporation *J. Phys. D: Appl. Phys.* **40** 3683–8

[10] Liu J, Wei A, Zhuang M and Zhao Y 2013 Investigation of the ZnS_xSe_{1-x} thin films prepared by chemical bath deposition *J. Mater. Sci.: Mater. Electron.* **24** 1348–53 (6)

[11] Ashraf M, Akhtar S M J, Mehmood M and Qayyum A 2009 Optical and structural properties of ZnS_xSe_{1-x} thin films deposited by thermal evaporation *Eur. Phys. J. Appl. Phys.* **48** 10501

[12] Valeev R G, Krylov P N and Romanov E A 2007 Structure and properties of ZnSe nanocomposite thin films *J. Surf. Investigation X-Ray Synchrotron Neutron Techn.* **1** 35–9

[13] Valeev R G, Romanov E A, Deev A, Beltukov A, Napolski K, Eliseev A, Krylov P N, Mezentsev N and Kriventsov V 2010 Synthesis of ZnSe semiconductor nanodot arrays by templated PVD *Phys. Status Solidi* C **7** 1539–41

[14] Valeev R, Romanov E, Beltukov A, Mukhgalin V, Roslyakov I and Eliseev A 2012 Structure and luminescence characteristics of ZnS nanodot array in porous anodic aluminum oxide *Phys. Status Solidi* C **9** 1462–5

[15] Sadovnikov S I, Kozhevnikova N S and Rempel A A 2010 The structure and optical properties of nanocrytalline lead sulfide films *Semiconductors* **44** 1349–56

[16] Valeev R G, Beltukov A N, Gilmutdinov F Z, Romanov Â A, Deev A N, Kriventsov V V, Mezentsev N A and Chukavin A I 2011 EXAFS spectroscopy study of the atomic structure of ZnS nanocomposite thin films *J. Struct. Chem.* **52** 181–5

[17] Maruyama T, Ogawa T, Akimoto K, Kitajima Y, Itoh S and Ishibashi A 1996 Distribution of chalcogen atoms in ZnSSe and ZnMgSSe: an EXAFS study *J. Cryst. Growth* **159** 41–4

[18] Glover J L and Chantler C T 2007 The analysis of x-ray absorption fine structure: beam-line independent interpretation *Meas. Sci. Technol.* **18** 2916–20

[19] Chaboy J, Garcia J, Marcelli A and Tyson T A 1993 On the amplitudes of EXAFS spectra at the L edges *Japan. J. Appl. Phys.* **32S2** (Supplement 32-2) 107–9

[20] Robouch B V, Kisiel A and Konior J 2002 Statistical model for site occupation preferences and shapes of elemental tetrahedra in the zinc-blende type semiconductors GaInAs, GaAsP, ZnCdTe *J. Alloys Compd.* **339** 1–17

[21] Robouch B V, Kisiel A and Konior J 2002 Statistical model for atomic distances and site occupation in zinc-blende diluted magnetic semiconductors (DMSs) *J. Alloys Compd.* **340** 13–26

[22] Robouch B V, Burattini E, Kisiel A, Suvorov A L and Zaluzhnyi A G 2003 Strained-tetrahedra statistical model for atomic distances and site occupations in ternary intermetallic $M_3(X\,X')$ structures $Ni_3(AlFe)$ case *J. Alloys Compd.* **359** 73–8

[23] Robouch B V, Sheregii E M and Kisiel A 2004 Statistical strained tetrahedron model of local ternary zinc blend crystal structures *Low Temp. Phys.* **30** 921–9

[24] Robouch B V, Sheregii E M and Kisiel A 2004 Statistical analysis of inter-ionic distances and occupation preferences in ternary zincblende and wurtzite structured crystals *11 Int. Conf. on Phonon Scattering in Condensed Matter—Phonons 2004 (St.Petersburg, Russia, July 25–30)* vol 1 *Physica Status Solidi* c pp 3015–8 idem: Report LNF-04/20 (P) 15.10.2004 pp.1-6

[25] Robouch B V *et al* 2011 Ion distribution preferences in ternary crystals $Zn_xCd_{1-x}Te$, $Zn_{1-x}Hg_xTe$ and $Cd_{1-x}Hg_xTe$ *Eur. Phys. J.* B **84** 183–95

[26] Abo-Hassan K M M, Muhamad M R and Radhakrishna S 2005 Some structural parameters of ZnS_xSe_{1-x} thin films prepared by electron beam evaporation *Physica* B **358** 256–64

[27] Gad S, Rafea M A and Badr Y 2012 Optical and photoconductive properties of $Pb_{0.9}Sn_{0.1}Se$ nano-structured thin films deposited by thermal vacuum evaporation and pulsed laser deposition *J. Alloys Compd.* **515** 101–7

[28] Xu H, Liang Y, Liu Z, Zhang X and Hark S 2008 Synthesis and optical properties of tetrapod-like ZnSSe alloy nanostructures *Adv. Mater.* **20** 3294–7

[29] Chang I F and Mitra S S 1968 Application of a modified random-element-isodisplacement model to long-wavelength optic phonons of mixed crystals *Phys. Rev.* **172** 924–33

[30] Hayashi K, Sawaki N and Akasaki I 1991 Raman scattering in ZnS_xSe_{1-x} alloys *Japan. J. Appl. Phys.* **30** 501–5

[31] Krylov P N, Gilmutdinov F Z, Romanov E A and Fedotova I V 2011 The influence of thermal annealing on the optical properties of nanocrystalline zinc sulfide films *Semiconductors* **45** 1512–6

[32] Lunz U, Schumacher C, Nürnberger J, Schüll K, Gerhard A, Schüssler U, Jobst B, Faschinger W and Landwehr G 1997 The energy gap Eg of $Zn_{1-x}Mn_xS_{1-y}Se_{1-x}$ epitaxial layers as a function of composition and temperature *Semicond. Sci. Technol.* **12** 970–3